Proceedings of the Institution of Mechanical Engineers, Part C: Journal of Mechanical Engineering Science
http://pic.sagepub.com/

Recent developments in exact strip analysis and optimum design of aerospace structures

D Kennedy, M Fischer and C A Featherston

Proceedings of the Institution of Mechanical Engineers, Part C: Journal of Mechanical Engineering Science 2007 221: 399
DOI: 10.1243/0954406JMES432

The online version of this article can be found at:
http://pic.sagepub.com/content/221/4/399

Published by:
SAGE
http://www.sagepublications.com

On behalf of:
Institution of Mechanical Engineers
Institution of Mechanical Engineers

Additional services and information for *Proceedings of the Institution of Mechanical Engineers, Part C: Journal of Mechanical Engineering Science* can be found at:

Email Alerts: http://pic.sagepub.com/cgi/alerts

Subscriptions: http://pic.sagepub.com/subscriptions

Reprints: http://www.sagepub.com/journalsReprints.nav

Permissions: http://www.sagepub.com/journalsPermissions.nav

Citations: http://pic.sagepub.com/content/221/4/399.refs.html

>> Version of Record - Apr 1, 2007

What is This?

Downloaded from pic.sagepub.com at Cardiff University on April 4, 2012

Recent developments in exact strip analysis and optimum design of aerospace structures

D Kennedy*, **M Fischer,** and **C A Featherston**
Cardiff School of Engineering, Cardiff University, Cardiff, UK

The manuscript was received on 30 June 2006 and was accepted after revision for publication on 23 January 2007.

DOI: 10.1243/0954406JMES432

Abstract: The current paper outlines recent developments to algorithms and software for critical buckling and natural vibration analysis and optimum design of prismatic plate assemblies, based on the exact strip approach and the Wittrick–Williams algorithm. The current paper acts as a single source document discussing recent progress and planned future explorations in: initial local postbuckling of stiffened panels; discrete optimization of composite structures to satisfy manufacturing requirements; discontinuous cost functions; constraints on fundamental natural frequencies and frequency-free bands; a feasibility study of response surface optimization; and multi-level optimization of composite aircraft wings. The numerous references provide fuller technical details and illustrative examples.

Keywords: aerospace structures, buckling, postbuckling, vibration, optimization

1 INTRODUCTION

The analysis and design of aerospace and lightweight structures are typically complex problems. In order to achieve high standards of operating efficiency, components need to be as light as possible, while at the same time a multitude of structural and other constraints need to be satisfied.

For many years, the finite-element method (FEM) [**1**–**3**] has provided a particularly versatile approach, allowing structures of great complexity to be analysed. However, this approach still often comes at an exceptionally high computational cost, particularly where repeated analysis is required, e.g. in iterative solutions of non-linear problems and in optimum design.

Although the FEM has been continuously developed, particularly in the context of commercial software solutions, to provide highly reliable means of analysis, simulation and design, most alternative methods and procedures have failed to mature, so that typically very expensive experiments are needed to verify analytical results and provide adequate benchmarking. In this context, alternative approaches such as the finite-strip method [**4**–**8**] have proved particularly valuable; in that precision and efficiency are enhanced by using an analytical solution in one direction.

Additionally, the modelling and computational costs of discretization can be avoided altogether by using analytical solutions of the governing differential equations [**9**, **10**]. This approximate analytical approach, which is exact for certain simple cases (e.g. prismatic assemblies of orthotropic rectangular plates with simply supported ends and no shear loading), is often referred to as the 'exact strip' method. For buckling and vibration problems it results in transcendental eigenproblems, rather than the linear ones resulting from FEM discretization of the structure.

Coupled with a highly efficient and extremely reliable algorithm [**11**, **12**], which ensures that any eigenvalue (i.e. critical buckling load or natural frequency of free vibration) can be found with absolute certainty, the exact strip method has been found to be much faster than the FEM for the analysis of prismatic plate structures [**13**]. Although advances in computational technology enable extremely large and complex structures to be analysed by special purpose FEM software, aerospace designers continue to seek faster, reliable alternatives, for example, to avoid

**Corresponding author: Cardiff School of Engineering, Cardiff University, Queen's Buildings, The Parade, Cardiff CF24 3AA, UK. email: kennedyd@cf.ac.uk*

Downloaded from pic.sagepub.com at Cardiff University on April 4, 2012

excessive modelling costs when carrying out parametric preliminary design studies, or for use in conjunction with FEM and optimization software when repeated analysis is required within a multi-level or multi-disciplinary design scenario.

The exact strip method forms the foundation of the specialist analysis and optimum design software VICONOPT [**13**] (subsequently referred to as 'the software'), which has been developed for typical aerospace structures, such as aircraft wing panels made from isotropic (e.g. metallic) or anisotropic (e.g. carbon-fibre composites and fibre-metal laminates) materials. However, while the software can analyse and design integral prismatic structural components, e.g. stiffened panels and wing boxes, it is unable to handle general three-dimensional structures subject to complex external loading. Typically, a finite-element analysis of the overall structural system is required to determine the loads acting on the individual components before they are analysed or optimized. Despite this limitation and some approximations necessary as a part of the modelling process, the software has been used for analysis and design purposes, in both industry and academia, for more than a decade.

Following recommendations made by the Group for Aeronautical Research and Technology in Europe during the 1990s [**14**], many enhancements have been made to further improve the software's exact strip analysis and optimum design capabilities. These include: the development of a geometrically nonlinear procedure for the local postbuckling analysis of perfect or imperfect longitudinally compressed plate assemblies [**15**]; the provision of discrete design capability [**16**]; discontinuous cost functions [**16**]; optimization with vibration constraints [**16**]; response surface applications [**17**]; and the development of a multi-level optimization interface linking the software with the finite-element solver MSC/NASTRAN [**18**].

The purpose of the current paper is to provide a single source document giving an overview of the recent developments that have taken place. The main theoretical principles involved are discussed, and references are made to papers giving more details and some practical applications. In the context of the issues discussed above, the future potential of the exact strip method and its likely benefits to the aerospace industry are explored.

2 THE EXACT STRIP METHOD AND WITTRICK–WILLIAMS ALGORITHM

The exact strip method assumes a continuous distribution of stiffness over the structure rather than discretized stiffnesses at nodal points, as is the case for the FEM. The method is based on analytical solutions to the partial differential equations, which (after any modelling assumptions) govern the in-plane and out-of-plane deformation of the component plates. Where possible, a closed form solution procedure [**19**] is used to determine the member stiffness matrices $\mathbf{k}_m$, which are subsequently assembled into the global stiffness matrix $\mathbf{K}$ for the overall structure. If a closed form solution of the member equations is not available the $\mathbf{k}_m$ matrices can be found by solving the member equations numerically [**20**]. The global stiffness matrix $\mathbf{K}$ relates a finite set of displacements $\boldsymbol{D}$ at the nodes of the structure to their corresponding perturbation forces $\boldsymbol{P}$, by

$$\mathbf{K}\boldsymbol{D} = \boldsymbol{P} \tag{1}$$

$\mathbf{K}$ consists of transcendental, and thus highly nonlinear, functions of the load factor F or frequency ω [**10**]. The critical buckling loads or natural frequencies of the structure correspond to the eigenvalues found by solving

$$\mathbf{K}\boldsymbol{D} = \boldsymbol{0} \tag{2}$$

The solution of the transcendental eigenvalue problem requires an iterative search for the values of F or ω at which equation (2) is satisfied. The software makes use of the Wittrick–Williams algorithm [**11**, **12**], which allows the eigenvalues to be found with absolute certainty. The algorithm calculates J, the number of eigenvalues lying between zero and any trial value of F or ω. Any change in J between two trial values is equal to the number of eigenvalues lying between these trial values.

In its general form the Wittrick–Williams algorithm can be stated as

$$J = J_0 + s\{\mathbf{K}\} \tag{3}$$

where $s\{\mathbf{K}\}$ is known as the sign count of $\mathbf{K}$, and corresponds to the number of negative leading diagonal elements of the upper triangular matrix $\mathbf{K}^{\Delta}$ obtained by applying conventional Gauss elimination, without pivoting, to the matrix $\mathbf{K}$. J_0 is the value that J would have if all the freedoms corresponding to $\mathbf{K}$ were fully restrained. Unless substructures are used, J_0 can be calculated as

$$J_0 = \sum_m J_m \tag{4}$$

where the summation is over all members m of the structure, and J_m is calculated for each member as the number of eigenvalues exceeded by the trial value when the member ends are fully restrained.

For computational efficiency, the algorithm allows the use of substructures. Their contribution to J_0 can

Downloaded from pic.sagepub.com at Cardiff University on April 4, 2012

be determined by prior application of the algorithm to each substructure, with all points of attachment between the substructure and parent structure clamped [**12**].

3 VICONOPT SOFTWARE

The VICONOPT software [**13**] incorporates the earlier programs VIPASA (vibration and instability of plate assemblies including shear and anisotropy) [**19**] and VICON (VIPASA with constraints) [**21**]. It covers elastic buckling, local postbuckling, and free vibration of prismatic plate assemblies, and provides an efficient design tool for structural optimization. In contrast to the conventional FEM, the software's exact strip analysis uses a transcendental stiffness matrix derived from analytical solutions of the governing differential equations of the component plates. For any longitudinally invariant loading combination (of longitudinal, transverse, in-plane shear, and pressure loads), critical buckling loads, undamped natural frequencies, and mode shapes can be found with certainty, using procedures based on the Wittrick–Williams algorithm [**11**, **12**]. Typical sections that the software can analyse, and a typical component plate showing in-plane loading, are shown in Figs 1 and 2. In the VIPASA analysis [**19**], the mode of buckling or vibration is assumed to vary sinusoidally in the longitudinal (x) direction, with a half-wavelength λ, which divides exactly into the panel length ℓ, so that exact solutions are obtained for simply supported isotropic and orthotropic panels without shear loading. For panels that are anisotropic or loaded in shear, the VICON analysis [**21**] couples such modes,

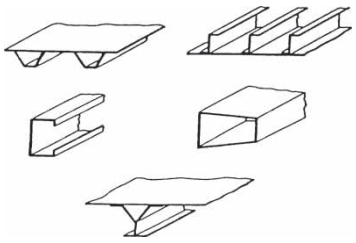

Fig. 1 Typical sections that VICONOPT can analyse

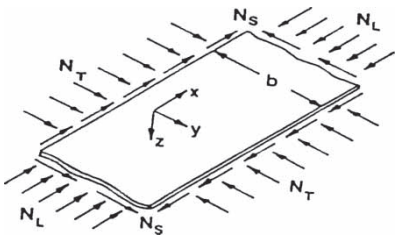

Fig. 2 Component plate, showing axis system and in-plane loading

using Lagrangian multipliers to approximate the end conditions.

4 LOCAL POSTBUCKLING ANALYSIS OF AEROSPACE STRUCTURES

Aerospace structures such as longitudinally stiffened panels can often carry loads far in excess of their critical buckling loads. This postbuckling reserve of strength is primarily because of stress redistributions within the structure following buckling in a local mode and, if allowed for in minimum mass design, can make a valuable contribution to the overall efficiency of such structures. However, with the onset of buckling, the growth of the out-of-plane deflections typically leads to significant stress redistributions across the overall structure, and the stiffness of any buckled component plates is reduced against further compression. It is important to note that such postbuckling behaviour is significantly influenced by geometric imperfections such as manufacturing faults.

An understanding of the postbuckling behaviour of a structure is essential, in order to fully optimize reserves by extending the design envelope as far as possible into the postbuckling region. Early analyses involved examination of the initial postbuckling behaviour of structures to provide more accurate estimates of critical loads for use in design. In the early 1940s von Karman *et al.* [**22**–**24**] showed that the large discrepancies between test and theory for the buckling of particular types of shell structures were because of their highly unstable postbuckling behaviour and worked to obtain an indication of the minimum load a structure could support in its buckled state to act as a design load, which would recognize this. In 1945, Koiter [**25**] elaborated the modern theory of structural stability for continuous elastic systems, which was further developed by Budiansky [**26**] and then Thompson [**27**] who used generalized coordinates to develop the general theory for discrete systems. In each of these theories, the emphasis was shifted to determine the maximum load, which could be supported by a structure before buckling was triggered, and to relate this load to the magnitude and forms of any imperfections present. Interest in the initial postbuckling approach increased significantly in the 1960s [**28**–**31**]. Since then, many studies have been carried out to determine the postbuckling behaviour of particular structures and these are summarized in reviews [**32**–**34**]. Significant themes have been the sensitivity of structures to geometric imperfections and load eccentricities [**35**, **36**], coupled instabilities [**37**–**40**], mode jumping [**41**, **42**], and plasticity [**43**]. More recently, this work has been extended to predict the behaviour

Downloaded from pic.sagepub.com at Cardiff University on April 4, 2012

much further into the postbuckling range in order to extend the design envelope towards collapse and to extend theory from homogeneous, metallic structures, to those made from newer materials such as fibre composites [**44**–**46**].

This section describes a geometrically non-linear procedure, which has been implemented within the limitations of the software, for the local postbuckling analysis of perfect or imperfect longitudinally compressed prismatic plate assemblies [**15**]. Areas of application will be outlined; fuller details being available in the references provided.

4.1 Theory

The exact strip analysis and the Wittrick–Williams algorithm presented in section 2 provide valuable opportunities for the postbuckling analysis of plate and shell structures. Using an iterative procedure, the software permits determination of the ratio of postbuckling to prebuckling axial stiffness K^*/K and the relationship between applied load P and the longitudinal end-shortening strain ε_x well into the postbuckling region. The overall accuracy of the postbuckling results is improved [**15**] by taking into account the stabilizing effects of the transverse tension developed in the central portion of a plate whose longitudinal edges are constrained to remain straight. The analysis is based on the assumption that the panel has simply supported ends, and buckles locally with a half-wavelength λ, which divides exactly into the panel length ℓ. The method allows for prismatic plate assemblies having a general cross-section. As illustrated in Fig. 3, a component plate of width b is divided into n_s longitudinal strips of equal width

$$b_s = \frac{b}{n_s} \tag{5}$$

The material properties can be either isotropic or anisotropic, and a uniform thickness t is assumed across each plate. The analysis optionally allows for initial geometric shape imperfections with maximum out-of-plane displacement γ_0. Restricting attention

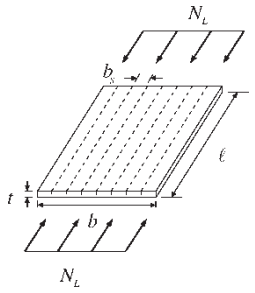

Fig. 3 Typical flat plate of width b, subdivided into n_s strips of width b_s

to a single plate (for simplicity), the initial stress resultants are calculated for each strip as

$$N_{xs} = N_{\mathrm{L}} = \frac{P}{b} \tag{6}$$

The iterative procedure of the non-linear analysis consists of a predefined number of cycles, each defined by a maximum out-of-plane displacement γ_2. At the start of each new cycle, γ_2 is incremented by a predefined amount. During each cycle, the applied load P and the longitudinal end-shortening strain ε_x, which correspond to the displacement γ_2, are determined. This process requires a number of iterations for convergence, because of changes in the postbuckling mode shape and the stress distributions across the cross-section of the structure.

At the start of each iteration, the buckling load P_c and mode shape (of amplitude γ_2) for a perfect structure with the present stress distribution are found. Imperfections are assumed to have the same shape as the buckling mode but for an amplitude of γ_0, so that the applied load P for the imperfect structure is

$$P = \left(1 - \frac{\gamma_0}{\gamma_2}\right) P_c \tag{7}$$

For the first iteration of the second and all subsequent cycles, the buckling load, mode shape, and applied load calculations are replaced by estimated values, derived from the converged results from the previous cycle.

The longitudinal strain due to the applied load P is P/S_1, where S_1 is defined in terms of the in-plane elastic properties A_{ij} by

$$S_1 = b\left(A_{11} - \frac{A_{12}^2}{A_{22}}\right) \tag{8}$$

The longitudinal strain ε_{x0} at the initial buckling load P_{c0} is thus given by

$$\varepsilon_{x0} = \frac{P_{c0}}{S_1} \tag{9}$$

For the plate shown in Fig. 4, the change in projected length of a linear element of length dx in the longitudinal direction due to an out-of-plane displacement w_2 is given by $(\partial w_2/\partial x)^2 \mathrm{d}x/2$. The flexural strain ε_{Fx} due to bending of an imperfect plate with half-wavelength λ is thus given, by considering the difference between the final and initial projected lengths, as

$$\varepsilon_{Fx} = \frac{1}{2\lambda}\int_0^{\lambda}\left[\left(\frac{\partial w_2}{\partial x}\right)^2 + \left(\frac{\partial v_2}{\partial x}\right)^2 - \left(\frac{\partial w_0}{\partial x}\right)^2 - \left(\frac{\partial v_0}{\partial x}\right)^2\right]\mathrm{d}x \tag{10}$$

Downloaded from pic.sagepub.com at Cardiff University on April 4, 2012

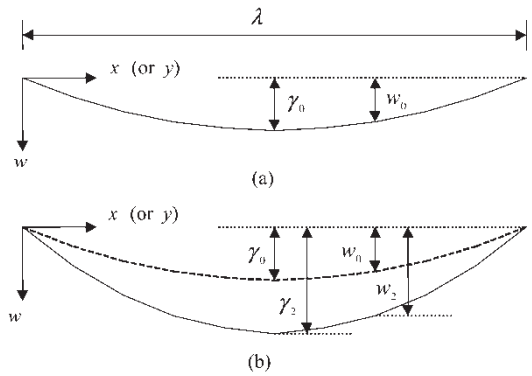

Fig. 4 Cross-section of a part of a thin rectangular plate having an initial imperfection w_0 with maximum value γ_0: (a) unloaded; (b) loaded

The displacement v (in the global y-direction) has been included in addition to w, to allow for the arbitrary alignment of plates in a stiffened panel.

Assuming sinusoidal variations of the modal displacements along any longitudinal line, so that

$$w_2 = \bar{w}_2 \sin(\pi x/\lambda) \tag{11}$$

equation (10) can be evaluated to give

$$\varepsilon_{Fx} = \left(\frac{\pi^2}{4\lambda^2}\right)(\bar{w}_2^2 + \bar{v}_2^2 - \bar{w}_0^2 - \bar{v}_0^2) \tag{12}$$

the overbars denoting the amplitudes. The stress resultant for flexure is then given by

$$N_{Fx} = \varepsilon_{Fx}\frac{S_1}{b} \tag{13}$$

After buckling has occurred, stress redistribution takes place in the plate, as illustrated in Fig. 5. The average stress resultant is $N_{\mathrm{L}}(=P/b)$. At the edges, the stress resultant due to flexure is zero and the stress is taken as $S_2\, N_{\mathrm{L}}$, where

$$S_2 = 1 + \left(\frac{1}{P}\right)\sum_s (b_s N_{Fxs}) \tag{14}$$

and N_{Fxs} is taken as the mean of the values of N_{Fx} at the two edges of strip s. The overall stress resultant N_{xs}

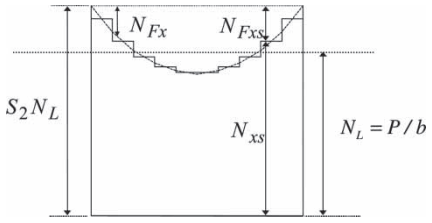

Fig. 5 Variation of stress resultants across a plate

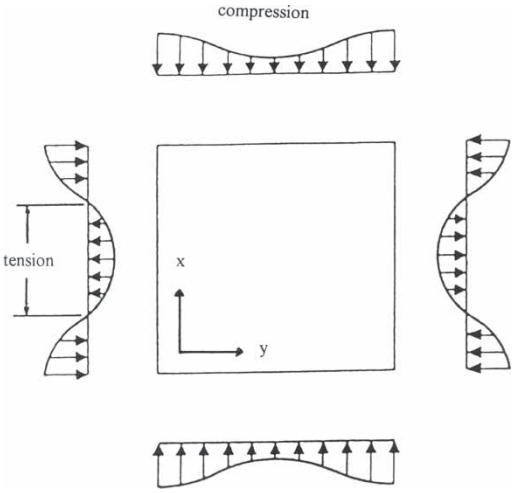

Fig. 6 Variation of stresses in a simply supported square plate whose longitudinal edges remain straight

in a strip is given by

$$N_{xs} = S_2 N_{\mathrm{L}} - N_{Fxs} \tag{15}$$

and the end-shortening strain ε_x due to the applied load and postbuckling mode is given by

$$\varepsilon_x = \frac{S_2 P}{S_1} \tag{16}$$

Note that if the plate is supported so that the longitudinal edges can move transversely but are required to remain straight, a transverse stress distribution develops as shown in Fig. 6. Tension and compression regions develop such that the resultant transverse load, obtained by integrating the transverse stress resultant along the length of the plate, remains zero. Because the compression regions occur close to the supported ends, while the tension region occurs in the central portion where $(\partial w_2/\partial y)$ is large, the transverse tension region proves to be the more important and provides a net stabilizing effect to the postbuckled plate. Taking such stabilizing effects into account improves the accuracy of the postbuckling analysis [**15**, **47**].

Convergence within each cycle is based on finding consistent estimates of P, ε_x, and N_{xs}. The ratios P/P_{c0} and $\varepsilon_x/\varepsilon_{x0}$ from each cycle are plotted to determine the ratio of postbuckling to prebuckling axial stiffness K^*/K.

Prior to the commencement of each new cycle, the imperfection shape is altered to that of the latest converged mode, representing the worst possible shape. Although the amplitude of the imperfection remains unaltered, the postbuckling mode is rescaled using an increased value of γ_2 for the maximum out-of-plane displacement. An estimated buckling load is then obtained by straight line extrapolation through

Downloaded from pic.sagepub.com at Cardiff University on April 4, 2012

the converged values of P_c and γ_2 from the last two cycles, and used in place of P_c in equation (7) to estimate the applied load for the first iteration of the next cycle.

4.2 Applications

The above procedure has been used for local postbuckling analyses of isotropic and anisotropic, perfect and imperfect, longitudinally compressed, plates and panels. Their convergence behaviour was studied, as were the effects of increasing transverse tension, imperfection sizes, and buckling mode changes [**15**, **47**].

Given the regular geometry of typical aerospace panels, it is often possible to divide the structure into repeating portions of identical geometry and to assume that these portions remain identically loaded. Because of the repetitive nature of the overall structure, it is then sufficient to analyse just one of the repeating portions. Case studies have been carried out [**15**, **47**, **48**] for the postbuckling behaviour of perfect isotropic and infinitely wide simply supported panels (Fig. 7(a)), curved panels (Fig. 7(b)), and longitudinally stiffened cylindrical shells (Fig. 7(c)). Although good agreement was obtained with previously published results, there is evidence that for some problems convergence can be impeded by limited numerical accuracy of the buckling modes, interaction between similar local modes and mode jumping. Mode accuracy has been improved for two-dimensional frame structures [**49**] by combining the Wittrick–Williams algorithm with a recursive Newton method involving inverse iteration, and it is planned to extend these ideas to the mode calculations of the postbuckling analysis. A preliminary study on mode jumping [**50**] has provided useful insights, which will lead to further analysis of advanced postbuckling behaviour.

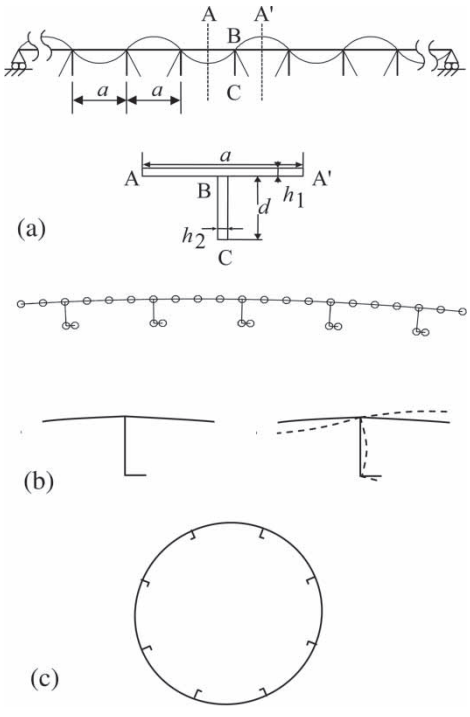

Fig. 7 Typical applications for postbuckling analysis: (a) cross-section of a perfect isotropic infinitely wide panel with simply supported ends, showing the local buckling mode, and dimensions of a typical repeating portion (ABCA′); (b) curved simply supported panel, showing repeating portion and local buckling mode; and (c) longitudinally stiffened cylindrical shell

5 OPTIMIZATION OF AEROSPACE STRUCTURES

The main objective of aerospace structural optimization is to design structures as light as possible without jeopardizing any safety requirements, e.g. to satisfy constraints on structural stability. Although the widely used FEM is very versatile, allowing structures with a wide range of loading and boundary conditions to be analysed, it comes at a very high computational cost. This is, particularly, the case when performing design optimization, which requires many finite-element analyses to be carried out.

The efficiency of such optimization tasks can be dramatically improved if the analyses are instead based on the exact strip method described in section 2. For more than a decade the software [**13**] has been used extensively [**51**] for the design of both isotropic and anisotropic structural components, such as aircraft wing panels. Possible design variables include the geometric dimensions of individual component plates, as well as individual layer thicknesses and ply orientations in the case of composite materials. Structures can be designed subject to initial buckling, material strength, overall stiffness, and/or geometric constraints, to provide minimum weight or to minimize an alternative cost function [**52**].

The following subsections describe recent enhancements to the design capability of the software, including discrete optimization [**16**], discontinuous cost functions [**16**], vibration constraints [**53**–**55**], and multi-level optimization [**18**, **56**]. A new optimization strategy based on response surfaces has also been explored [**17**].

5.1 Continuous optimization

The continuous design phase (CDP) is based on the sizing strategy of steps 1–8 and 12 in Fig. 8. Any set $\boldsymbol{x} = \{x_j, j = 1, \ldots, n\}$ of plate widths, layer thicknesses

Downloaded from pic.sagepub.com at Cardiff University on April 4, 2012

and ply orientations may be chosen as independent design variables, while other dimensions may be held fixed or linked to the design variables. Sizing is performed (step 5) using the mathematical programming optimizer CONMIN [**57**], together with a stabilization (i.e. thickness factoring) procedure [**51**] (steps 2 and 6), which achieves a just stable configuration. Move limits are adjusted intelligently by the program (step 4). Because the stiffness matrix varies transcendentally with the load factor, the buckling sensitivities cannot easily be obtained analytically and so are found (step 3) by an efficient estimation technique [**51**].

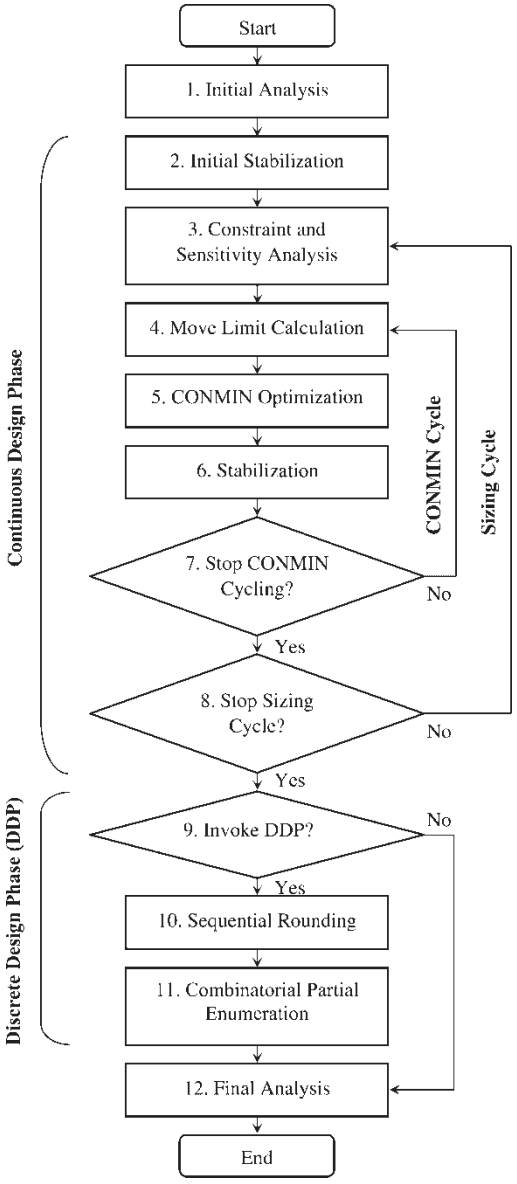

Fig. 8 Panel design strategy showing the continuous and discrete design phases

5.2 Discrete optimization

Steps 9 to 12 in Fig. 8 cover the extensions made to the software in order to allow discrete optimization. This new discrete design phase (DDP) [**16**] is intended to provide rapid convergence on practical panel configurations satisfying discrete manufacturing constraints. It, therefore, follows the continuous phase, using the final continuous design as a starting configuration $(\boldsymbol{x}_{\mathrm{C}}, f_{\mathrm{C}})$ having design variables $\boldsymbol{x}_{\mathrm{C}}$ and objective function value f_{C}. The DDP encompasses a two-stage process for convergence to an adjacent feasible discrete solution $(\hat{\boldsymbol{x}}, \hat{f})$. The objective function f to be minimized (e.g. panel mass) is here assumed to vary monotonically with each of the discrete design variables.

The first stage of the DDP uses a simple sequential rounding technique (SRT) to determine an initial feasible discrete solution. The SRT is made up of a sequence of three separate steps. The first step identifies all the d ($\leqslant n$) discrete design variables $x_{\mathrm{D}j}$ ($j = 1, \ldots, d$) from $\boldsymbol{x}$ and rounds them from their continuous values $x_{\mathrm{C}j}$ down to their next lower discrete values $x^{-}_{\mathrm{D}j}$. The second step ranks the variables in descending order of the sensitivities of the objective function with respect to each variable, by perturbing the variable values in turn from $x^{-}_{\mathrm{D}j}$ to the next upper discrete value $x^{+}_{\mathrm{D}j}$. In the final step, the design configuration is checked for stability following successive adjustment of each discrete variable $x_{\mathrm{D}j}$ in turn (according to rank) from $x^{-}_{\mathrm{D}j}$ to $x^{+}_{\mathrm{D}j}$. The adjustments are continued until the first stable configuration is achieved. The design $(\hat{\boldsymbol{x}}, \hat{f})$ thus obtained becomes an incumbent upper bound solution $(\boldsymbol{x}^{\mathrm{U}}, f^{\mathrm{U}})$ for the second stage of the DDP. The continuous design $(\boldsymbol{x}_{\mathrm{C}}, f_{\mathrm{C}})$ is made the lower bound solution $(\boldsymbol{x}^{\mathrm{L}}, f^{\mathrm{L}})$.

Once upper and lower bound solutions have been established, the second stage of the DDP is entered. This stage is based upon the binary enumeration tree concept involving branching and fathoming of nodes [**58**]. The nodes serve as intermediate steps to achieving configurations in which the variables $x_{\mathrm{D}j}$ all take appropriate discrete values. From each node at level j, two descendant nodes are generated at which variable $x_{\mathrm{D}j}$ is restricted to take the values $x^{-}_{\mathrm{D}j}$ and $x^{+}_{\mathrm{D}j}$, respectively. The complete discrete configurations are only attained at level d of the enumeration tree, yielding a combinatorial problem of size 2^d.

The decision to branch from a typical node k is subject to the outcome of a feasibility test. The test requires the determination of lower (f^{-}_{k}) and upper (f^{+}_{k}) limits for the objective function value at descendants of node k. The initial limits f^{-}_{0} and f^{+}_{0} are calculated using the sensitivities found in the first stage of the DDP; the limits are successively tightened at subsequent levels as variables are fixed to their discrete values $x^{-}_{\mathrm{D}j}$ and $x^{+}_{\mathrm{D}j}$. The limits f^{-}_{k} and

Downloaded from pic.sagepub.com at Cardiff University on April 4, 2012

f_k^+ are checked against the global bounds f^{L} and f^{U}. Node branching is only continued if both (a) $f_k^+ \geqslant f^{\mathrm{L}}$ and (b) $f_k^- \leqslant f^{\mathrm{U}}$. Otherwise, node k is abandoned as either (a) infeasible or (b) unable to improve on the incumbent solution. Descendant configurations of such fathomed nodes are thus implicitly disregarded.

Each candidate design at level d is abandoned if f exceeds the incumbent value $\hat{f}$. Otherwise the design is checked for stability by a single iteration of the Wittrick–Williams algorithm [**11**] and, if found to be feasible (i.e. if $J = 0$ in equation (3)), becomes the new incumbent solution $(\hat{\boldsymbol{x}}, \hat{f})$. The enumeration procedure terminates when all outstanding nodes have been branched on or abandoned, at which point the incumbent design $(\hat{\boldsymbol{x}}, \hat{f})$ is declared as the optimal discrete solution of the problem adjacent to the continuous solution $(\boldsymbol{x}_{\mathrm{C}}, f_{\mathrm{C}})$ previously determined by the CDP.

Important aerospace applications include the design of metallic plate structures with a specified discrete set of permissible plate thicknesses, and the design of laminated composite structures, where each layer must comprise an integer number of plies of a standard thickness [**59**]. Illustrative examples [**16**] demonstrate substantial mass savings over the simple expedient of rounding up of every discrete design variable from its value at the continuous optimum to the next permitted discrete value. A recent study [**60**] has demonstrated the feasibility of continuing the branching in pursuit of the global discrete optimum solution. Areas for future work include the discrete optimization problems associated with ply angle selection and stacking sequence design.

5.3 Discontinuous cost functions

Next, an innovative approach is proposed, enabling the software to solve optimization problems possessing discontinuous cost functions, which may vary non-monotonically with the design variables at the discontinuities [**16**]. Any gradient-based optimizer will clearly have difficulty in predicting objective function values and slopes for design moves that straddle such discontinuities. It has been established that if the software is applied to such problems in the conventional way, the generation of search directions within the linear optimizer is severely compromised. As a result, the program is unable to traverse the discontinuities intelligently, thus preventing the location of an optimum design.

The new strategy entails a systematic consideration of the different regions of the design space separated by the discontinuities in the cost functions. Partitioning of the design space into regions is, in fact, necessary to handle these discontinuities. The suggested approach does not require the introduction of a new optimization technique, but rather repeats the existing strategy of the software over the different partitions of the design space. For simplicity the objective function is assumed to comprise discontinuous 'stepped' cost functions, each of a single 'stepped' design variable. The main features include classification of the stepped cost function types, stepped variable position checks and alteration of variable limits, to be used in additional 'CONMIN procedures', which each comprise a number of the CONMIN cycles of steps 4 to 7 of Fig. 8.

Each sizing cycle commences with a CONMIN procedure (i.e. a number of CONMIN cycles) in which moves are permitted throughout the design space, i.e. the steps in the cost function are ignored. The program automatically updates and retains the best design it has encountered so far, which is assumed to be locally optimal within its own region, i.e. a step must be crossed in order to reach any better solution. By calculating appropriate function values and gradients, each of the stepped cost functions is now classified according to whether each step represents an increase or decrease in the function value and whether the gradient is positive or negative immediately above and below the step. By checking the positions of the stepped variables against this classification, it is possible to determine whether a better solution can occur in any adjacent region. If so, an additional CONMIN procedure is initiated, in which the bounds of one of the stepped variables are adjusted so as to restrict attention to this adjacent region. For example, to force a variable upwards across a step, its lower bound is set to the position of the step and its upper bound is set to the user-specified upper bound, or to the position of the next step in the cost function (if there is one). Bounds for the remaining design variables are set by the usual move limit calculations of step 4 of Fig. 8. The starting configuration for the additional CONMIN procedure is that of the best design found so far, with the stepped variable shifted to the bound at the step across which it has been forced.

Further CONMIN procedures are performed to ensure a search over all regions likely to contain improving solutions, the best solution found over the whole sizing cycle being retained. The optimization process terminates if no further improvement is made from one sizing cycle to the next, or if the difference between the objective function values at the ends of two consecutive sizing cycles is within a specified tolerance.

The method has been evaluated by the optimization of stiffened panels with arbitrary discontinuous cost functions of varying complexity [**16**, **59**].

Downloaded from pic.sagepub.com at Cardiff University on April 4, 2012

5.4 Optimization with vibration constraints

Previously, the optimization strategy of the software [**13**] primarily considered buckling and material strength constraints [**51**]. Fundamental natural frequency constraints and frequency free band constraints have now been incorporated into this strategy.

As before, a stabilization procedure (steps 2 and 6 of Fig. 8) is used in conjunction with the linear optimizer to obtain a just feasible configuration. However, in contrast to buckling design situations, simply factoring the plate thicknesses does not ensure that the fundamental natural frequency will shift monotonically and rapidly. Thus a revised method of stabilization is now used to guarantee accurate convergence on a stabilized design having a fundamental natural frequency chosen by the designer. The revised method factors both layer thicknesses and the widths of the plates containing the layers (provided the widths have also been declared as design variables). The amount by which each plate width is factored is governed by the factor, which is applied to each layer thickness until an upper or lower bound is reached. If the total thickness of a plate is thus factored by $\bar{F}$ then the plate width is factored by $\bar{F}^{\alpha}$, where $0.1 \leqslant \alpha \leqslant 0.4$. This valid range of α has been determined by analytical consideration of the effects of thickness and width factoring for various modes of vibration [**53**].

The above method of stabilization ensures monotonic behaviour with respect to buckling, material strength, overall stiffness, geometric, and fundamental natural frequency constraints. However, a further important practical requirement is the creation of frequency free bands [**55**] and such constraints are ignored by the method thus far described. A consequence is that, although the linear optimizer attempts to move natural frequencies out of a band, the stabilization procedure could force them back into the band. Thus it is desirable that the linear optimizer produces a design for which stabilization requires minimal thickness and width factoring, and where the frequencies have been shifted a reasonable distance beyond the band limits specified by the designer. The design move made by the optimizer is guided by the sensitivities, which are defined as approximate (and appropriately normalized) partial derivatives of the natural frequency with respect to the design variables. Typically some natural frequencies will increase while others decrease. The intention here is to force all natural frequencies initially in the lower half of the required band downwards and to force those in the upper half upwards, while also considering all other constraints and minimizing mass.

In practise, more than one frequency free band constraint may be specified, and it may not always be possible for the optimizer to locate a design where all such constraints are satisfied. In such cases, a search is employed to find other frequency free bands of sufficient width that may be shifted into the position of the specified band locations. Such bands must always be shifted upwards to avoid violating the fundamental frequency constraint. Mass is, therefore, added as though stabilization had been further employed to obtain a design where the fundamental frequency constraint is not critical. Stabilization is not an optimizing step, and a severe mass penalty can be incurred if the optimizer does not easily find a solution.

The strategic positioning of discrete scalar quantities of mass on a structure's surface has the beneficial effect of forcing sound to be radiated less efficiently [**61**]. Strategic point mass positioning could also be used to shift natural frequencies away from one or more forcing frequencies, although obtaining an overall optimum design is dependent upon the position of nodal lines of higher frequencies [**62**]. Ideally the optimal solution is to position the point masses at the locations of greatest out-of-plane displacement. This is not always possible since the region above the intended frequency free band could be of high spectral density, possibly involving frequencies of different longitudinal and transverse half-wavelengths.

The software can now produce an optimum design with specified frequency free bands. However, if the actual load and/or edge conditions are different from those modelled, the structure's stiffness will inevitably change and thus frequencies will shift, perhaps becoming unacceptably close to the forcing frequency. In this case, non-load carrying point masses could be added efficiently to redefine the band. The software uses a variant of its Lagrangian multiplier analysis to calculate the natural frequencies and mode shapes of such structures [**63**].

Illustrative results have been obtained [**16**, **53**–**55**] for a range of stiffened panel examples including fundamental natural frequency and frequency free band constraints.

5.5 Response surface optimization

Response surface methodology [**64**] comprises a number of mathematical and statistical techniques used to approximate the relationship between a response (output) variable and a number of design (input) variables. The intention is not to determine the underlying physical relationships, but to approximate them locally by fitting a multi-dimensional surface through a discrete set of sampling points. Analytical optimization of the surface then provides an approximately optimal solution to the physical problem. The methodology is commonly used in the pure and

Downloaded from pic.sagepub.com at Cardiff University on April 4, 2012

applied sciences, and is increasingly being applied to structural optimization [**65**].

Figure 9 shows schematic contour plots of natural frequencies for an isotropic blade-stiffened panel of aerospace proportions, for a range of values of (non-dimensional) skin thickness t_1 and stiffener thickness t_2. The plots were obtained [**17**] by interpolation through natural frequencies found by the software [**13**] at the 36 grid points shown, and cover local, overall and torsional modes of vibration. For the local mode, the contour plot of Fig. 9(a) shows that the natural frequency increases monotonically with both t_1 and t_2. This plot appears to be quite suitable for the gradient-based optimization of the software, and closely resembles the corresponding plot of the critical buckling load. In contrast, for the overall and torsional modes represented by Figs 9(b) and (c), respectively, there is non-monotonic behaviour, which could cause serious difficulties in gradient-based optimization.

Polynomial response surfaces were fitted to the data of Fig. 9 using unweighted least squares regression. For example, the coefficients $c_1, \ldots, c_6$ for a quadratic surface

$$F(t_1, t_2) = c_1 + c_2 t_1 + c_3 t_2 + c_4 t_1^2 + c_5 t_1 t_2 + c_6 t_2^2 \quad (17)$$

were found by minimizing

$$\sum_{i=1}^{n} [F(t_{1i}, t_{2i}) - f_i]^2 \quad (18)$$

the sum of squares of the discrepancies between the fitted function $F(t_1, t_2)$ and the data values f_i at the n data points $t_1 = t_{1i}$, $t_2 = t_{2i}$ $(i = 1, \ldots, n)$. Such a quadratic response surface gave a good approximation to the actual behaviour of Fig. 9(a), while for Figs 9(b) and (c), a cubic response surface was needed to obtain appropriate accuracy.

A great advantage of using polynomial response surface models to represent natural frequency constraints during structural optimization is that many computationally intensive natural frequency calculations can be avoided. Indeed, the optimization of the surface can be carried out independently of the structural analysis software, and for the present work this was performed using the Solver optimizer of Microsoft Excel [**66**]. Illustrative results [**17**] gave errors of the order of 1 per cent between the actual natural frequencies and those predicted by the response surface.

As a refinement, the 'zooming' strategy of Fig. 10 was adopted, using the software MATLAB [**67**], and was shown [**17**] to improve accuracy by adding more sampling points in the vicinity of the supposed optimum. Further algorithmic refinements [**64**] are desirable for problems with larger numbers of design variables, so as to keep the number of sampling points and polynomial coefficients in manageable proportions. A similar approach has recently led to increased understanding of the initial buckling of aircraft wing spars under combined loading [**68**].

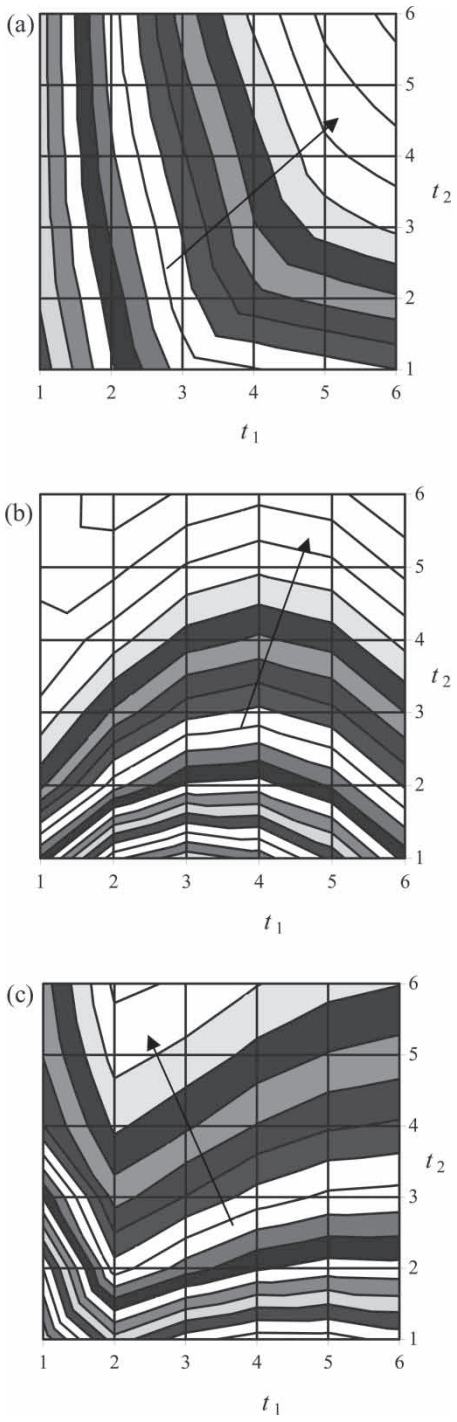

Fig. 9 Schematic contour plots of natural frequencies against non-dimensional skin thickness t_1 and stiffener thickness t_2 for a blade-stiffened panel: (a) local mode; (b) overall mode; and (c) torsional mode; the arrows denote increasing natural frequencies

Downloaded from pic.sagepub.com at Cardiff University on April 4, 2012

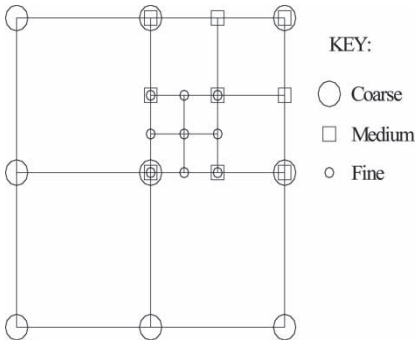

Fig. 10 Illustration of 'zooming' strategy, showing coarse, medium, and fine level grids over a two-dimensional design space

5.6 Multi-level optimization

The software interface Viconopt MLO [**18**, **56**] has been developed for the multi-level optimization of lightweight structures, such as composite aircraft wings. By means of a robust and easy-to-use windows interface, the software links one of the most widely used finite element solvers, MSC/NASTRAN [**69**], with the fast and efficient design capabilities of the VICONOPT software [**13**]. MSC/NASTRAN models of entire plate assemblies are readily translated into a panel format by Viconopt MLO. Using the MSC/NASTRAN input file and initial results from an existing finite-element model, panel optimization models are generated for each of the component plates (or assemblies thereof). Most of the software's existing analysis and design features have been implemented in Viconopt MLO for user selection.

The iterative multi-level optimization process is based on the interaction between models at the MSC/NASTRAN and VICONOPT levels. These two levels are commonly referred to as system level and panel level, respectively. In the current version of Viconopt MLO, design changes are only made at panel level, and are automatically fed back into the finite-element model at system level. Because of these design changes the load carrying capacity of the overall structure is altered and stress redistributions must be determined at the beginning of each new multi-level optimization cycle. The panel level models are then updated and the process is repeated until an overall mass convergence criterion is met.

In addition to providing an interface for multi-level optimization, Viconopt MLO is currently being developed as a pre/postprocessor for conventional panel level models. These can either be generated from scratch or imported from system level models. Where panel level models have been imported from system level models, any additional parameters necessary for a panel analysis or optimization can be specified in Viconopt MLO. This approach completely avoids the need for text input files to be generated manually, so that models can be assembled, analysed and optimized much more quickly and efficiently.

Figure 11 gives a detailed flowchart representation of the multi-level optimization procedure adopted by Viconopt MLO. It is important to note that the software interfaces directly with MSC/NASTRAN, making the procedures for the data transfer independent of any pre/postprocessor used to generate the system level model. The present implementation uses MSC/PATRAN [**70**].

Once a MSC/NASTRAN model has been generated for the overall structure at system level, an initial finite-element analysis is carried out in order to determine the internal stress distribution across the

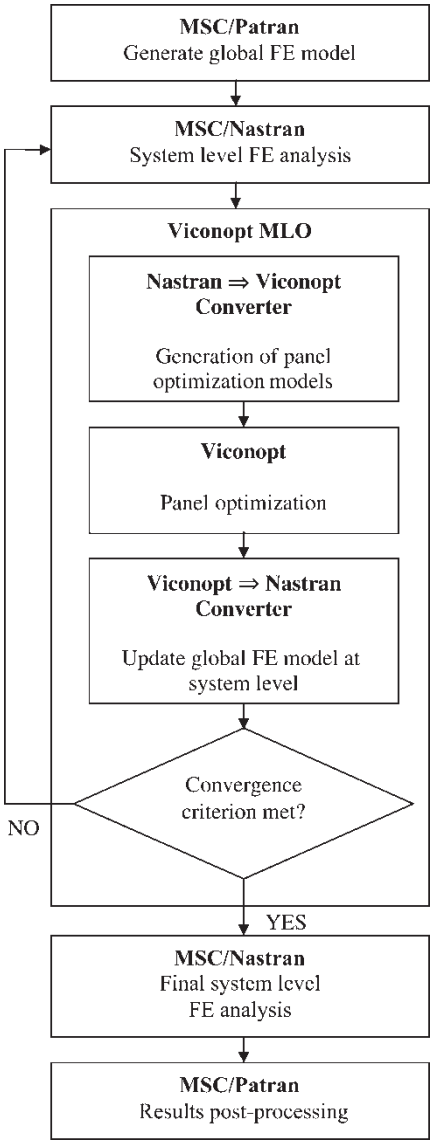

Fig. 11 Flowchart of multi-level optimization procedure in Viconopt MLO

Downloaded from pic.sagepub.com at Cardiff University on April 4, 2012

structure. All the structural components that constitute plates in a panel level model must be modelled as plates at the system level and must be assigned their individual property cards, so that all the model information required to specify the optimization problem at the panel level can be translated by the 'NASTRAN to VICONOPT' converter in Viconopt MLO. Any additional parameters required to create the panel models may be specified using the preprocessing capabilities of Viconopt MLO.

When all the panel level models have been created, Viconopt MLO automatically generates the VICONOPT input files needed to analyse and optimize each of the panels separately.

The next stage uses the 'VICONOPT to NASTRAN' converter to feed all the design changes made to the panels back into the original finite-element model, which is subsequently re-analysed. A new system level finite-element analysis is carried out, and the stress redistributions resulting from the design changes are determined. All the panel level models are updated and re-optimized. Viconopt MLO repeats the above procedure until a final convergence criterion on the overall mass of the structure is satisfied (e.g. <1 per cent change in mass between successive cycles).

A case study has been recently carried out for a composite aircraft wing consisting of 12 panels, for which a total of 144 design variables were defined. The multilevel process showed good convergence behaviour, in terms of both mass and stress redistribution following the design changes [**18**, **71**]. Although only relatively simple problems have been solved to date, there is potential for further development, including the possibility of links to alternative finite-element software and specialist panel codes.

6 CONCLUSIONS

The exact strip approach provides an attractive alternative to the conventional FEM for the analysis of a range of isotropic and anisotropic prismatic plate assemblies, including typical aircraft wing and fuselage panels. By using the Wittrick–Williams algorithm, structural eigenvalues, i.e. critical buckling loads, and natural frequencies of free vibration, can be found with certainty. This approach is central to the software VICONOPT, in which the eigenvalue analysis is coupled with gradient-based optimization tools to minimize the structural mass (or an alternative cost function).

Recent analytical developments to the software include the extension of the critical buckling analysis into the initial local postbuckling range. The consequent non-uniform longitudinal stress distribution is approximated by dividing each component plate into strips, whereas the transverse stress is modelled by introducing an empirical tension factor.

The continuous optimum design capability of the software has been extended by adjusting the optimal values of the design variables to adjacent discrete values, e.g. in order to satisfy manufacturing requirements for composites where each layer thickness must be an integer multiple of a standard ply thickness. The adjustments are made locally, by sequential rounding and binary branching, after the continuous optimization and they incur a relatively small mass penalty.

Other optimum design developments include special algorithms to handle discontinuous cost functions, as well as constraints on the fundamental natural frequency and the removal of all natural frequencies from specified frequency bands. Optimization has also been performed efficiently by approximating the constraints using response surfaces.

Finally, VICONOPT has been linked with the finite-element software MSC/NASTRAN to form a powerful tool for the multi-level optimization of a complete aircraft wing.

ACKNOWLEDGEMENTS

The work presented in this paper has been funded by Airbus UK, NASA Langley Research Center, the Engineering and Physical Sciences Research Council, Universities UK Overseas Research Students Awards Scheme Committee, and Cardiff University. Cardiff University students, including O. J. O'Leary, T. J. Ong, S. M. Powell, and L. J. Townsend, made significant technical contributions.

REFERENCES

1 **Courant, R.** Variational methods for the solution of problems of equilibrium and vibrations. *Bull. Am. Math. Soc.*, 1943, **49**(1), 1–23.
2 **Turner, M. J., Clough, R. W., Martin, H. C.,** and **Topp, L. C.** Stiffness and deflection analysis of complex structures. *J. Aero. Sci.*, 1956, **23**(9), 805–823.
3 **Zienkiewicz, O. C.** *The finite element method*, 1977 (McGraw-Hill, London).
4 **Kantorovich, L. V.** and **Krylov, V. I.** *Approximate methods of higher analysis*, 1958 (Noordhoff, Groningen).
5 **Cheung, Y. K.** The finite strip method in the analysis of elastic plates with two opposite simply supported ends. *Proc. Inst. Civ. Eng.*, 1968, **40**(1), 1–7.
6 **Cheung, M. S., Cheung, Y. K.,** and **Ghali, A.** Analysis of slab and girder bridges by the finite strip method. *Bldg. Sci.*, 1970, **5**(2), 95–104.
7 **Plank, R. J.** and **Wittrick, W. H.** Buckling under combined loading of thin, flat-walled structures by a complex finite strip method. *Int. J. Numer. Methods Eng.*, 1974, **8**(2), 323–339.

Downloaded from pic.sagepub.com at Cardiff University on April 4, 2012

8 **Dawe, D. J.** Finite strip buckling analysis of curved plate assemblies under biaxial loading. *Int. J. Solids Struct.*, 1977, **13**(11), 1141–1155.

9 **Wittrick, W. H.** A unified approach to the initial buckling of stiffened panels in compression. *Aero. Q.*, 1968, **24**(3), 265–282.

10 **Williams, F. W.** and **Wittrick, W. H.** Computational procedures for a matrix analysis of the stability and vibration of thin flat-walled structures in compression. *Int. J. Mech. Sci.*, 1969, **11**(12), 979–998.

11 **Wittrick, W. H.** and **Williams, F. W.** A general algorithm for computing natural frequencies of elastic structures. *Q. J. Mech. Appl. Math.*, 1971, **24**(3), 263–284.

12 **Wittrick, W. H.** and **Williams, F. W.** An algorithm for computing critical buckling loads of elastic structures. *J. Struct. Mech.*, 1973, **1**(4), 497–518.

13 **Williams, F. W., Kennedy, D., Butler, R.,** and **Anderson, M. S.** VICONOPT: program for exact vibration and buckling analysis or design of prismatic plate assemblies. *AIAA J.*, 1991, **29**(11), 1927–1928.

14 **DERA.** *Final report of the GARTEUR action group on structural optimisation SM(AG13)*, vols 1–3, 1997 (DERA, Farnborough).

15 **Powell, S. M., Williams, F. W., Askar, A.-S.,** and **Kennedy, D.** Local postbuckling analysis for perfect and imperfect longitudinally compressed plates and panels. In Proceedings of the 39th AIAA/ASME/ASCE/AHS/ASC Structures, Structural Dynamics and Materials Conference, Long Beach, CA, 1998, Pt I, pp. 595–603 (AIAA, Reston, VA).

16 **Kennedy, D., Ong, T. J., O'Leary, O. J.,** and **Williams, F. W.** Practical optimisation of aerospace panels. In Proceedings of the 1st ASMO UK/ISSMO Conference, Ilkley, 1999, pp. 217–224 (MCB University Press, Bradford).

17 **Townsend, L. J.** and **Kennedy, D.** Optimum design of stiffened panels with vibration constraints using response surface modelling. In Proceedings of the 2nd ASMO UK/ISSMO Conference, Swansea, 2000, pp. 219–226 (University of Wales, Swansea).

18 **Fischer, M., Kennedy, D.,** and **Featherston, C. A.** Multilevel optimization of a composite aircraft wing using Viconopt MLO. In Proceedings of the 9th AIAA/ISSMO Symposium on *Multidisciplinary analysis and optimization*, Atlanta, GA, 2002, paper AIAA 2002-5511 (AIAA, Reston, VA).

19 **Wittrick, W. H.** and **Williams, F. W.** Buckling and vibration of anisotropic or isotropic plate assemblies under combined loadings. *Int. J. Mech. Sci.*, 1974, **16**(4), 209–239.

20 **Anderson, M. S.** and **Kennedy, D.** Transverse shear deformation in exact buckling and vibration analysis of composite plate assemblies. *AIAA J.*, 1993, **31**(10), 1963–1965.

21 **Anderson, M. S., Williams, F. W.,** and **Wright, C. J.** Buckling and vibration of any prismatic assembly of shear and compression loaded anisotropic plates with an arbitrary supporting structure. *Int. J. Mech. Sci.*, 1983, **25**(8), 585–596.

22 **von Karman, T.** and **Tsien, H. S.** The buckling of spherical shells by external pressure. *J. Aero. Sci.*, 1939, **7**, 43–50.

23 **von Karman, T., Dunn, L. G.,** and **Tsien, H. S.** The influence of curvature on the buckling characteristics of structures. *J. Aero. Sci.*, 1940, **7**, 276–289.

24 **von Karman, T.** and **Tsien, H. S.** The buckling of thin cylindrical shells under axial compression. *J. Aero. Sci.*, 1941, **8**, 303–312.

25 **Koiter, W. T.** *Over de stabiliteit van het elastisch evenwicht (On the stability of elastic equilibrium)*. PhD Thesis, University of Delft, 1945. English translation issued as NASA TT F-10, 833, 1967.

26 **Budiansky, B.** Theory of buckling and postbuckling behaviour of elastic structures. In *Advances in applied mechanics* (Ed. C. S. Yih), vol. 14, 1974, pp. 1–65 (Academic Press, New York).

27 **Thompson, J. M. T.** Basic principles in the general theory of elastic stability. *J. Mech. Phys. Solids*, 1963, **11**(1), 13–20.

28 **Chilver, A. H.** Coupled modes of elastic buckling. *J. Mech. Phys. Solids*, 1967, **15**(1), 15–28.

29 **Thompson, J. M. T.** The estimation of elastic critical loads. *J. Mech. Phys. Solids*, 1967, **15**, 311–317.

30 **Walker, A. C.** An analytical study of the rotationally symmetric nonlinear buckling of a complete spherical shell under external pressure. *Int. J. Mech. Sci.*, 1968, **10**, 695–710.

31 **Sewell, M. J.** A general theory of equilibrium paths through critical points. *Proc. R. Soc.*, 1968, **A306**(Pt I), 201–223; (Pt II), 225–238.

32 **Thompson, J. M. T.** A general theory for the equilibrium and stability of discrete conservative systems. *J. Appl. Math. Phys. (ZAMP)*, 1969, **20**, 797–846.

33 **Hutchinson, J. W.** and **Koiter, W. T.** Postbuckling theory. *Appl. Mech. Rev.*, 1970, **23**(12), 1353–1366.

34 **Gioncu, V.** General theory of coupled instabilities. *Thin-Walled Struct.*, 1994, **19**(2–4), 81–127.

35 **Singer, J., Baruch, M.,** and **Harari, O.** On the stability of eccentrically stiffened cylindrical shells under axial compression. *Int. J. Solids Struct.*, 1967, **3**, 445–470.

36 **Arbocz, J.** and **Babcock, C. D.** The effect of general imperfections on the buckling of cylindrical shells. *J. Appl. Mech.*, 1969, **36**(1), 28–38.

37 **Thompson, J. M. T.** and **Hunt, G. W.** A theory for the numerical analysis of compound branching. *J. Appl. Math. Phys. (ZAMP)*, 1971, **22**, 1001–1015.

38 **Thompson, J. M. T.** and **Hunt, G. W.** *A general theory of elastic stability*, 1973 (Wiley, London).

39 **Tvergaard, V.** Imperfection sensitivity of a wide integrally stiffened panel under compression. *Int. J. Solids Struct.*, 1973, **9**(1), 177–192.

40 **van der Neut, A.** Mode interaction with stiffened panels. In *Buckling of structures* (Ed. B. Budiansky), 1974, pp. 117–131 (Springer-Verlag, Berlin).

41 **Supple, W. J.** Changes of wave-forms of plates in the postbuckling range. *Int. J. Solids Struct.*, 1970, **6**, 1243–1258.

42 **Bushnell, D.** Optimization of stiffened panels in which mode jumping is accounted for. In Proceedings of the 38th AIAA/ASME/ASCE/AHS/ASC Structures, Structural Dynamics and Materials Conference, Kissimmee, FL, 1997, Pt III, pp. 2123–2162 (AIAA, Reston, VA).

Downloaded from pic.sagepub.com at Cardiff University on April 4, 2012

43 Graves Smith, T. R. The ultimate strength of thin-walled columns of arbitrary length. In *Thin walled steel structures* (Eds K. C. Rockey and H. V. Hill), 1969, pp. 35–60 (Crosby Lockwood, London).

44 van Houten, M. H. and **Zdunek, A.** *Post-buckling and collapse analysis*, final technical report, GARTEUR SM(AG25) TP-149, 2004.

45 Zimmermann, R. and **Rolfes, R.** POSICOSS – improved postbuckling simulation for design of fibre composite stiffened fuselage structures. *Compos. Struct.*, 2006, **73**(2), 171–174.

46 Degenhardt, R., Rolfes, R., Zimmermann, R., and **Rohwer, K.** COCOMAT – improved material exploitation of composite airframe structures by accurate simulation of postbuckling and collapse. *Compos. Struct.*, 2006, **73**(2), 175–178.

47 Powell, S. M. *Buckling and postbuckling of prismatic plate assemblies using exact eigenvalue theory*. PhD Thesis, University of Wales, Cardiff, 1997, pp. 105–155.

48 Fischer, M. and **Kennedy, D.** Local postbuckling analysis of curved aerospace structures. In Proceedings of the 22nd International Congress of Aeronautical Sciences, Harrogate, 2000, pp. 423.1–423.10 (Optimage, Edinburgh).

49 Yuan, S., Ye, K., Williams, F. W., and **Kennedy, D.** Recursive second order convergence method for natural frequencies and modes when using dynamic stiffness matrices. *Int. J. Numer. Methods Eng.*, 2003, **56**(12), 1795–1814.

50 Watson, A. and **Kennedy, D.** Mode jumping in post-buckled stiffened panels. In Proceedings of the 4th International Conference on Thin-Walled Structures, Loughborough, 2004, pp. 573–580 (Institute of Physics Publication, Bristol).

51 Butler, R. and **Williams, F. W.** Optimum design using VICONOPT, a buckling and strength constraint program for prismatic assemblies of anisotropic plates. *Comput. Struct.*, 1992, **43**(4), 699–708.

52 Edwards, D. A. Cost optimization of stiffened panels using VICONOPT. *AIAA J.*, 1998, **36**(2), 267–272.

53 O'Leary, O. J. *Optimisation of prismatic plate structures with natural frequency constraints*. PhD Thesis, University of Wales, Cardiff, 2000.

54 O'Leary, O. J., Williams, F. W., and **Kennedy, D.** Optimum stiffened panel design with fundamental frequency constraint. *Thin-Walled Struct.*, 2001, **39**(7), 555–569.

55 Kennedy, D., O'Leary, O. J., and **Williams, F. W.** Optimum design of prismatic plate assemblies with spectral gap constraints. In Proceedings of the 5th International Symposium on Vibrations of Continuous Systems, Berchtesgaden, 2005, pp. 36–38 (Virginia Polytechnic Institute and State University, Blacksburg, VA).

56 Fischer, M., Kennedy, D., and **Featherston, C. A.** Multilevel optimization of aerospace and lightweight structures. In Proceedings of the 23rd International Congress of Aeronautical Sciences, Toronto, 2002, pp. 344.1–344.9 (Canadian Aeronautics and Space Institution, Ottawa).

57 Vanderplaats, G. N. and **Moses, F.** Structural optimization by methods of feasible directions. *Comput. Struct.*, 1973, **3**(4), 739–755.

58 Garfinkel, R. S. and **Nemhauser, G. L.** *Integer programming*, 1972 (Wiley, New York).

59 Ong, T. J. *Practical optimisation of lightweight structures*. PhD Thesis, University of Wales, Cardiff, 2000.

60 Kennedy, D., Ioannidis, G., and **Featherston, C. A.** Discrete optimum design of composite plates including longitudinal voids. In Proceedings of the 6th World Congress on *Computational mechanics* in conjuction with 2nd Asian-Pacific Congress on Computational Mechanics, Beijing, 2004, paper M636, pp. 1–10 (Tsinghua University Press, Beijing).

61 St Pierre, R. L., Jr and **Koopmann, G. H.** A design method for minimizing the sound power radiated from plates by adding optimally sized, discrete masses. *Trans. ASME, J. Mech. Des.*, 1995, **117B**, 243–251.

62 McMillan, A. J. and **Keane, A. J.** Shifting resonances from a frequency band by applying concentrated masses to a thin rectangular plate. *J. Sound Vib.*, 1996, **192**(2), 549–562.

63 Bennett, P. N. and **Williams, F. W.** Wave propagation along prismatic plate structures with masses attached by springs. In Proceedings of the 6th International Conference on Recent Advances in Structural Dynamics, Southampton, 1997, vol. 3, pp. 1–16 (Univ. Southampton).

64 Box, G. E. P. and **Draper, N. R.** *Empirical model-building and response surfaces*, 1987 (Wiley, New York).

65 Toropov, V. V., van Keulen, F., Markine, V. L., and **Alvarez, L. F.** Multipoint approximations based on response surface fitting: a summary of recent developments. In Proceedings of the 1st ASMO UK/ISSMO Conference, Ilkley, 1999, pp. 371–380 (MCB University Press, Bradford).

66 *Microsoft Corporation, Microsoft Excel Solver: user's guide*, 1980 (Microsoft, Redmond, WA).

67 Hahn, B. D. *Essential MATLAB for scientists and engineers*, 1997 (Arnold, London).

68 Featherston, C. A., Kennedy, D., Weston, D. A., and **Koffi, K.** Design rules for panel buckling under combined shear, compression and bending. In Proceedings of the 4th International Conference on Thin-Walled Structures, Loughborough, 2004, pp. 153–160 (Institute of Physics Publication, Bristol).

69 *MSC/Software, MSC/NASTRAN version 70.7*, 1999 (MSC, Los Angeles, CA).

70 *MSC/Software, MSC/PATRAN version 9.0*, 1999 (MSC, Los Angeles, CA).

71 Fischer, M. *Multilevel optimisation of aerospace and lightweight structures*. PhD Thesis, University of Wales, Cardiff, 2002, pp. 121–131.

APPENDIX

Notation

A_{ij}	in-plane elastic properties
b, b_s	width of plate, longitudinal strip
$c_1, \ldots, c_6$	response surface coefficients
d	number of discrete design variables
$\mathrm{d}x$	length of linear element
$\boldsymbol{D}$	vector of global displacements

Downloaded from pic.sagepub.com at Cardiff University on April 4, 2012

f	objective function
f_k^-, f_k^+	lower and upper objective function value limits at descendants of node k
F	load factor
$F(t_1, t_2)$	polynomial response surface
$\bar{F}, \bar{F}^\alpha$	total plate thickness factor, plate breadth thickness factor
j, k	enumeration tree level, node
J	number of eigenvalues lying between zero and a trial value
J_m	number of eigenvalues lying between zero and a trial value for a constituent member of a structure with its ends clamped
J_0	value of J when the components of the displacement vector corresponding to **K** are clamped
$\mathbf{k}_m$	member stiffness matrix
$\mathbf{K}$	global stiffness matrix
K, K^*	prebuckling, postbuckling axial stiffness
$\mathbf{K}^\Delta$	upper triangular matrix obtained by applying conventional Gauss elimination to **K**
ℓ	element length
n	number of design variables, number of data points
n_s	number of longitudinal strips of a component plate
N_{Fx}, N_{Fxs}	stress resultant for flexure of a component plate, plate strip
$N_\mathrm{L}, N_\mathrm{T}, N_\mathrm{S}$	longitudinal, transverse, shear in-plane loading components
N_{xs}	initial strip stress resultant
$\boldsymbol{P}$	vector of global perturbation forces
P, P_c	applied load, buckling load
P_{c0}	initial value of P_c
$s\{\mathbf{K}\}$	sign count of **K**, calculated as the number of negative elements on the leading diagonal of $\mathbf{K}^\Delta$
S_1, S_2	see equations (8) and (14)
t	component plate thickness
t_1, t_2	skin, stiffener thicknesses
v_0, v_2	initial and subsequent out-of-plane displacements in the global y direction
$\bar{v}_0, \bar{v}_2$	amplitudes of out-of-plane displacement in the global y direction
w_0, w_2	initial and subsequent out-of-plane displacements in the global z direction
$\bar{w}_0, \bar{w}_2$	amplitudes of out-of-plane displacement in the global z direction
x, y, z	global coordinate axes
$\boldsymbol{x} = \{x_j\}$	vector of independent design variables
$\hat{\boldsymbol{x}}, \hat{f}$	feasible discrete design solution (design variable values, objective function value)
$\boldsymbol{x}_\mathrm{C}, f_\mathrm{C}$	starting configuration for DDP (final continuous design, objective function value)
$x_{\mathrm{C}j}$	initial continuous values of discrete design variables $x_{\mathrm{D}j}$
$x_{\mathrm{D}j}$	discrete design variables ($j = 1, \ldots, d$)
$x_{\mathrm{D}j}^-, x_{\mathrm{D}j}^+$	nearest lower, upper discrete design variable values
$\boldsymbol{x}^\mathrm{L}, f^\mathrm{L}$	lower bound solution (design variable values, objective function value)
$\boldsymbol{x}^\mathrm{U}, f^\mathrm{U}$	upper bound solution (design variable values, objective function value)
γ_0	maximum out-of-plane displacement because of initial imperfection
γ_2	maximum out-of-plane displacement allowed per postbuckling analysis cycle
$\varepsilon_{Fx}, \varepsilon_x$	flexural strain, longitudinal end shortening strain
ε_{x0}	initial value of ε_x
λ	half-wavelength
ω	frequency

Downloaded from pic.sagepub.com at Cardiff University on April 4, 2012